Atmospheric Environment xxx (2011) 1–14

Contents lists available at ScienceDirect

Atmospheric Environment

journal homepage: www.elsevier.com/locate/atmosenv

Evaluation of sun photometer capabilities for retrievals of aerosol optical depth at high latitudes: The POLAR-AOD intercomparison campaigns

M. Mazzola [a,*], R.S. Stone [b,c], A. Herber [d], C. Tomasi [a], A. Lupi [a], V. Vitale [a], C. Lanconelli [a], C. Toledano [e], V.E. Cachorro [e], N.T. O'Neill [f,1], M. Shiobara [g], V. Aaltonen [h], K. Stebel [i], T. Zielinski [j], T. Petelski [j], J.P. Ortiz de Galisteo [e,k], B. Torres [e], A. Berjon [e], P. Goloub [l], Z. Li [l], L. Blarel [l], I. Abboud [m], E. Cuevas [n], M. Stock [o], K.-H. Schulz [p], A. Virkkula [h,q]

[a] Institute of Atmospheric Sciences and Climate, CNR, c/o ISAC-CNR, Via Gobetti 101, 40129 Bologna, Italy
[b] Cooperative Institute for Research in Environmental Sciences, University of Colorado at Boulder, Boulder, Colorado, USA
[c] Global Monitoring Division, Earth Systems Research Laboratory, National Oceanic and Atmospheric Administration, Boulder, Colorado, USA
[d] Climate Sciences, Alfred Wegener Institute for Polar and Marine Research, Bremerhaven, Germany
[e] Group of Atmospheric Optics, University of Valladolid, Valladolid, Spain
[f] Centre d'Applications et de Recherches en Télédétection, Université de Sherbrooke, Sherbrooke, QC, Canada
[g] National Institute of Polar Research, Tokyo, Japan
[h] Finnish Meteorological Institute, Helsinki, Finland
[i] Polar Environmental Centre, Norwegian Institute for Air Research, Tromsø, Norway
[j] Institute of Oceanology, Polish Academy of Sciences, Sopot, Poland
[k] Spanish Meteorological Agency (AEMET), Valladolid, Spain
[l] LOA, Université de Lille 1, CNRS, Lille, France
[m] Environment Canada, Experimental Studies Division, Toronto, Canada
[n] Izaña Observatory, Spanish Meteorological Agency (AEMET), Tenerife, Spain
[o] Climate Sciences, Alfred Wegener Institute for Polar and Marine Research, Potsdam, Germany
[p] Dr. Schulz & Partner GmbH, Buckow, Germany
[q] Department of Physics, University of Helsinki, Helsinki, Finland

ARTICLE INFO

Article history:
Received 7 April 2011
Received in revised form
21 July 2011
Accepted 24 July 2011

Keywords:
Aerosol
Polar regions
Sun photometry
Optical depth
Intercomparison
Calibration

ABSTRACT

Accuracy requirements for aerosol optical depth (AOD) in polar regions are much more stringent than those usually encountered in established sun photometer networks, while comparability of data from different archive centres is a further important issue. Therefore, two intercomparison campaigns were held during spring 2006 at Ny-Ålesund (Svalbard) and autumn 2008 at Izaña (Tenerife) within the framework of the IPY POLAR-AOD project, with the participation of various research institutions routinely employing different instrument models at Arctic and Antarctic stations. As reported here, a common algorithm was used for data analysis with the aim of minimizing a large part of the discrepancies affecting the previous studies. During the Ny-Ålesund campaign, spectral values of AOD derived from measurements taken with different instruments were found to agree, presenting at both 500 nm and 870 nm wavelengths average values of root mean square difference (RMSD) and standard deviation of the difference (SDD) equal to 0.003. Correspondingly, the mean bias difference (MBD) varied mainly between −0.003 and +0.003 at 500 nm, and between −0.004 and +0.003 at 870 nm. During the Izaña campaign, which was also intended as an intercalibration opportunity, RMSD and SDD values were estimated to be equal to 0.002 for both channels on average, with MBD ranging between −0.004 and +0.004 at 500 nm and between −0.002 and +0.003 at 870 nm. RMSD and SDD values for Ångström exponent α were estimated equal to 0.06 during the Ny-Ålesund campaign and 0.39 at Izaña. The results confirmed that sun photometry is a valid technique for aerosol monitoring in the pristine atmospheric turbidity conditions usually observed at high latitudes.

* Corresponding author. Tel.: +39 051 6399592; fax: +39 051 6399652.
E-mail address: m.mazzola@isac.cnr.it (M. Mazzola).
[1] On sabbatical leave for 2010/2011 at Department of Physics & Atmospheric Science, Dalhousie University, Halifax, NS, Canada.

1352-2310/$ – see front matter © 2011 Elsevier Ltd. All rights reserved.
doi:10.1016/j.atmosenv.2011.07.042

1. Introduction

The surface-atmosphere system conditions observed in polar regions (high surface albedo and low Sun elevation angles) greatly strengthen aerosol-induced effects on the radiation budget, contributing to modify the overall albedo of the Earth-atmosphere system (Shaw et al., 1993). Despite the important role of aerosols, the knowledge of their physical and radiative properties, horizontal and vertical mass concentration distributions, and temporal variability remains inadequate (Forster et al., 2007). Surface-based (in-situ, photometric, lidar) measurements allow the achievement of detailed and accurate results, and constitute a unique way of obtaining reliable information on aerosol radiative properties over highly reflective snow- and ice-covered surfaces, even if observing stations in polar regions are still few and far between.

Sun photometry is a useful tool for obtaining information on the optical and physical properties of aerosols along the atmospheric vertical path (Dubovik and King, 2000). In the past decade, sun photometric networks have been developed all over the world, including AERONET (Holben et al., 1998), GAW-PFR (Wehrli, 2000), SKYNET (Kim et al., 2004), and SURFRAD (Augustine et al., 2000). These networks have an almost global coverage, but only a few stations provide measurements with continuity at high latitudes (Stone, 2002; Herber et al., 2002; Rozwadowska and Sobolewski, 2010). Because of the low aerosol concentration usually observed and low solar elevation angles, the acquisition of accurate aerosol optical depth (AOD) measurements by means of sun photometers is in general difficult at high-latitude sites. The contributions of molecular scattering and absorption to the total optical depth (TOD) need to be evaluated as accurately as possible, because their values are often comparable or greater than AOD (Ortiz de Galisteo et al., 2008). The correct evaluation of the solar zenith angle (SZA) is of great importance in calculating the relative constituent-dependent optical air mass (m). In fact, atmospheric light refraction increases with SZA, while the different vertical profiles of the various atmospheric components variably influence calculations of m (Reagan et al., 1986). Instrument calibration is another major issue. It is usually performed by applying the Bouguer–Lambert–Beer law in Eq. (1) to data-sets collected over a sufficiently wide range of m, at least from 2 to 5. The higher the latitude of the site, the narrower is the range of diurnal variation of m during a given period. For this reason, it is not easy to calibrate such instruments with accuracy at polar sites.

The POLAR-AOD programme was proposed to the ICSU/WMO Joint Committee for the International Polar Year (IPY), with the aim of developing studies on the direct effects of polar aerosols on climate, and establishing a bipolar network of spectral radiometers to characterize their optical properties (see *http://classic.ipy.org/development/eoi/details.php?id=299*, and Tomasi et al., 2007). Two field campaigns were planned and carried out as a basic part of the POLAR-AOD project, the first at Ny-Ålesund (Spitsbergen, Svalbard archipelago, Norway) in early spring 2006 and the second at Izaña (Tenerife, Canary Islands, Spain) in October 2008.

Dealing with these issues, several comparison studies have been developed in recent years. Kim et al. (2008) intercompared measurements of AOD performed at various sites worldwide over long periods from about 1 to 3 years, finding that Sun-pointing instruments provide AOD (500 nm) values that agree within ±0.01 in terms of mean bias difference (MBD), for estimates of root-mean-square difference (RMSD) and standard deviation of difference (SDD) varying between less than 0.01 and 0.04 (see caption of Table 2 for definitions of the cited statistical parameters). The subsequent comparison of these results with those obtained from previous intensive studies provided the following statistic evaluations: (i) absolute values of MBD < 0.005 and SDD within the 0.001 - 0.005 range, for all the wavelengths considered (500, 670, 780, 870 and 1020 nm), from the 3-month measurements performed at Alice Springs and Tinga Tingana (Australia) using a pair of CIMEL and SP01A sun photometers in the first campaign, and a pair of CIMEL models in the second (Mitchell and Forgan, 2003); (ii) MBD values within ±0.006 at 380, 450, 870, and 1020 nm, and within ±0.010 at 525 nm, with RMSD ranging between 0.006 and 0.012, and SDD values between 0.006 and 0.011, from measurements taken at the ARM-SGP facility (Oklahoma, USA) using an Ames Airborne Tracking sun photometer (AATS-6) and a CIMEL sun photometer during a 15-day campaign (Schmid et al., 1999); (iii) absolute values of MBD < 0.007 at different wavelengths, and RMSD values < 0.01 from an intercomparison of three sun photometers (CIMEL, PFR and SP01A models) at the Bratt's Lake Observatory (Canada) (McArthur et al., 2003).

Such results suggest that intercomparison activities are very useful for limiting the discrepancies of the AOD evaluations obtained at the various wavelengths using different sun photometers. The description of the results obtained in the Ny-Ålesund and Izaña campaigns is the primary objective of the present work. Section 2 describes the field activities and provides details of the adopted methodologies. The overall precision of AOD is estimated from the field measurements (Sections 3.1 and 3.2), and the spectral dependence of AOD is evaluated in terms of the Ångström exponent α (Section 3.3). A detailed description of the calibration results obtained at Izaña is given in Section 3.2.1, while the comparison of the results with those available in the literature is made in Section 4. Finally, recommendations for obtaining accurate and comparable AOD measurements are made in Section 5.

2. Technical characteristics of the instruments employed in the POLAR-AOD campaigns

The main characteristics of the instruments employed during the two campaigns are listed in Table 1. Different radiometer models were used by the participating institutions: (i) CIMEL CE318 sun/sky-radiometer, the standard instrument of the AERONET network (Holben et al., 1998) and its sub-networks AEROCAN, PHOTONS and RIMA; (ii) PREDE POM02 sun/sky-radiometer, adopted by the SKYNET network (Kim et al., 2004); (iii) Precision Filter Radiometer (PFR), designed by the Swiss Physikalisch-Meteorologisches Observatorium Davos World Radiation Center (PMOD/WRC) and used in the World Meteorological Organization Global Atmospheric Watch (WMO/GAW) network (Wehrli, 2000); (iv) Carter–Scott SP01A and SP02 models, used by the Australian Bureau of Meteorology in its national network (Mitchell and Forgan, 2003) and by the National Oceanic & Atmospheric Administration/Global Monitoring Division (NOAA/GMD); (v) SP1A sun photometer, manufactured by Dr. Schulz & Partner GmbH and operated by the Alfred Wegener Institute for Polar and Marine Research (AWI) at their Antarctic and Arctic stations (Herber et al., 2002); (vi) ASP-15WL, designed at the Institute of Atmospheric Sciences and Climate (ISAC) of the Italian National Research Council (CNR), and deployed at the Italian Terra Nova Bay station (Antarctica) during summer campaigns (Tomasi et al., 2007). Alongside the above fully automated instruments, some hand-held MICROTOPS II sun photometers of Solar Light Company Inc. were operated during the two campaigns, this instrument being particularly suitable for itinerant campaigns or harsh environmental conditions, since it does not require the use of solar trackers and data acquisition systems (Smirnov et al., 2011). Their results were evaluated separately from that of the sun-tracking instruments, and were not utilized in the final evaluations of uncertainty parameters, because, as will be shown, precision achievable with

Please cite this article in press as: Mazzola, M., et al., Evaluation of sun photometer capabilities for retrievals of aerosol optical depth at high latitudes: The POLAR-AOD intercomparison campaigns, Atmospheric Environment (2011), doi:10.1016/j.atmosenv.2011.07.042

Table 1
Characteristics of the instruments employed in the two POLAR-AOD intercomparison campaigns.

Instrument	Institution	Location	Spectral range (nm) and number of filters	FOV (deg)	Acquisition rate (min)	Sun-tracking method	Thermal control	POLAR-AOD campaign
CIMEL CE-318	University of Sherbrooke, AEROCAN	Eureka	340–1640 (9)	1	3 (or air mass steps)	Built-in active tracker	Signal compensation	NYA(1), IZO(3)
CIMEL CE-318	University of Valladolid, RIMA	Andenes	340–1640 (9)	1	15 (or air mass steps)	Built-in active tracker	Signal compensation	NYA, IZO
CIMEL CE-318	AEMET	Izaña	340–1640 (9)	1	15 (or air mass steps)	Built-in active tracker	Signal compensation	IZO
CIMEL CE-318	University of Lille, PHOTONS	–	340–1640 (9)	1	15 (or air mass steps)	Built-in active tracker	Signal compensation	IZO
Dr. Schulz & Partner SP1A	AWI	Neumayer, Ny-Ålesund	349–1065 (17)	1	1	Dr. Schulz & Partner SPTR active tracker	None	NYA(2), IZO(2)
PMOD/WRC PFR	NILU	Troll, Ny-Ålesund	368–862 (4)	2.5	1	Kipp & Zonen astronomic tracker	Peltier cells	NYA
PMOD/WRC PFR	FMI	Jokioinen, Sodankylä	368–862 (4)	2.5	1	Kipp & Zonen astronomic tracker	Peltier cells	NYA, IZO
Carter-Scott SP01-A	NOAA/GMD	Barrow	413–865 (4)	2.4	1	Kipp & Zonen astronomic tracker	Built-in heater	NYA
Carter-Scott SP02	NOAA/GMD	South Pole	411–862 (4)	5	1	Kipp & Zonen astronomic tracker	Built-in heater	NYA
Carter-Scott SP02	NOAA/GMD	Terra Nova Bay, Dome C, campaigns	368–1050 (8)	5	1	Kipp & Zonen astronomic tracker	Built-in heater	IZO
ASP-15WL	ISAC	Terra Nova Bay	321–1026 (15)	1.1	1	Custom active tracker	Built-in heater	NYA
PREDE POM02	NIPR	Ny-Ålesund	315–2200 (11)	1	1 (or air mass steps)	Built-in active tracker	Built-in heater	NYA, IZO
PREDE POM02	ISAC	San Pietro Capofiume (Italy)	315–2200 (11)	1	1 min or air mass steps	Built-in active tracker	Built-in heater	IZO
Solar Light MICROTOPS II	IOPAS	Hornsund	340–1020 (6)	2.5	Variable	Hand-held	None	NYA(2), IZO(2)
Solar Light MICROTOPS II	University of Warsaw	Spitsbergen (cruises)	340–1020 (6)	2.5	Variable	Hand-held	None	IZO
Solar Light MICROTOPS II	FMI	ABOA	380–870 (5)	2.5	Variable	Hand-held	None	NYA, IZO

this kind of instruments is not sufficiently high for AOD retrievals in polar regions.

2.1. Measurement sites and methodologies

The first POLAR-AOD intercomparison campaign was performed at Ny-Ålesund (78° 55′ N, 11° 56′ E, Svalbard Islands, Norway) from March 25 to April 5, 2006, near the Rabben station of the National Institute of Polar Research (NIPR, Japan). It was organized and hosted by the AWI German station, using the instruments listed in Table 1 and labeled with the acronym NYA.

The second POLAR-AOD campaign was held from October 6–20, 2008, at the Izaña Observatory, a facility of the Centro de Investigación Atmosférico de Izaña (CIAI, *http://www.izana.org*) of the Spanish AEMET Agency (Agencia Estatal de Meteorología), located on the island of Tenerife (28° 19′ N, 16° 30′ W, 2360 m a.s.l., Canary Islands, Spain), 300 km from the West African coast. The instruments used during this intercomparison campaign are listed in Table 1 and labeled with the acronym IZO.

The spectral values of AOD were determined by inversion of the well known Bouguer–Lambert–Beer law

$$J(\lambda) = J_0(\lambda)R^{-2}e^{-m\tau(\lambda)}, \tag{1}$$

where $J(\lambda)$ is the measured signal, $J_0(\lambda)$ the corresponding extra-terrestrial value, i.e. the calibration constant, R is the solar distance expressed in astronomical units, m is the relative optical air mass and $\tau(\lambda)$ the total optical depth of the atmosphere. The last quantity can be written as the sum of the contributions due to different atmospheric constituents, as follows:

$$m\tau(\lambda) = m_a\tau_a(\lambda) + m_R\tau_R(\lambda) + m_G\tau_G(\lambda), \tag{2}$$

where $\tau_a(\lambda)$ is the aerosol optical depth, $\tau_R(\lambda)$ the Rayleigh-scattering optical depth, $\tau_G(\lambda)$ the gaseous absorption optical depth, and m_a, m_R, and m_G are the respective relative optical air masses. The above parameters are usually evaluated using the algorithms given in numerous works available in the literature (see Ortiz de Galisteo et al., 2008; Tomasi et al., 2005 for a complete list of references).

It is easy to verify in Eq. (1) that for low solar elevation angles, i.e. for high values of m, the measured signal is less influenced by the value of $J_0(\lambda)$. Similarly, AOD values obtained through Eq. (1) are less affected by errors made in evaluating the other variables. In fact, examining Eq. (1), and bearing in mind the propagation theory of errors, the absolute error of $\tau_a(\lambda)$ is given by

$$\Delta\tau_a(\lambda) = 1/m[\Delta m\tau_a(\lambda) + \Delta J(\lambda)/J(\lambda) + \Delta J_0(\lambda)/J_0(\lambda)] + \Delta\tau_R(\lambda) + \Delta\tau_G(\lambda), \tag{3}$$

where Δx represents the absolute error of each variable or term in Eqs. (1) and (2) (Reagan et al., 1986), and the first term given by the inverse of m is responsible for the decrease of error $\Delta\tau_a(\lambda)$ as m increases.

During the "WMO/GAW expert workshop on a global surface network for long-term observations of column aerosol optical properties" (WMO, 2005), a set of recommendations was formulated for the intercomparison campaigns. More than 1000 data points with AOD at 500 nm between 0.04 and 0.20 should be acquired over a minimum of 5 days, while the traceability requires 95% uncertainty within $0.005 + 0.01/m$ (U_{95}, International Organization for Standardization, 1995). The WMO experts also recommended the use of the 500 ± 3 nm and 865 ± 5 nm channels, with a bandwidth of 15 nm or less, as the basis for any sun photometer intercomparison and standard Ångström exponent (Ångström, 1964) evaluations, since such channels are largely free

Please cite this article in press as: Mazzola, M., et al., Evaluation of sun photometer capabilities for retrievals of aerosol optical depth at high latitudes: The POLAR-AOD intercomparison campaigns, Atmospheric Environment (2011), doi:10.1016/j.atmosenv.2011.07.042

from variable (water vapor and nitrogen dioxide) and strong (ozone) absorption effects. The AOD accuracy declared for the AERONET measurements is ±0.01 at wavelengths > 500 nm and ±0.02 at the shorter ones, made for average values of *m* (Holben et al., 2001).

3. Results

The results obtained from the analysis of the Ny-Ålesund and Izaña measurements are presented in the following sub-sections.

3.1. Ny-Ålesund intercomparison campaign

The Ny-Ålesund measurements were performed mainly from March 26 to March 31, 2006, providing more than 3200 coincident data points, i.e. about 400 per day on average. As can be seen in Fig. 1, AOD (500 nm) varied mainly between 0.08 and 0.20, being typical for the atmospheric turbidity conditions at the site at this time of the year (Tomasi et al., 2007). The campaign was planned with the principal aim of quantifying the comparability level among different and independent sun photometric measurements currently performed at stations worldwide. This was achieved through the two following steps: (i) comparing the evaluations made by different groups for the various terms of Eqs. (1) and (2), and (ii) putting together the raw voltages and values of J_0 assigned by each group, and running the data analysis employing a common algorithm, also for analyzing the causes of further discrepancies in AOD (e.g. calibration issues and/or instrumental characteristics).

In the first step, each group was requested to supply the values of Rayleigh-scattering optical depth (ROD), ozone optical depth (OOD) and SZA used in the data analysis, together with the set of ancillary parameters (local measurements, satellite data, climatology). It was verified that: (a) ROD assumed values of ~0.145 at 500 nm, which ranged within ±0.002 for the different algorithms employed by the different groups. It is worth noting that most of the groups adopted the algorithm proposed by Bodhaine et al. (1999) for the ROD corrections, while the AWI and NIPR used that of Fröhlich and Shaw (1980); (b) the values of OOD at 500 nm furnished by the various groups ranged within ±0.002 for fixed columnar contents of ozone, with average values varying between 0.011 and 0.015 on different days, with the only exception of the value used by the Norwegian Institute for Air Research (NILU) group, which was much higher and fixed at 0.031, due to the use of only one fixed climatological value of ozone total content; (c) discrepancies were found among the used SZA values, since the range of variability was typically 5′, yielding differences in the AOD estimates of 0.001–0.003 (Ortiz de Galisteo et al., 2008).

In the second step, an overall algorithm was used, including the Rayleigh-scattering of Bodhaine et al. (1999) and the ozone absorption coefficients given by the MODTRAN radiative transfer code (Berk et al., 2003). Following the suggestions of the WMO experts, the analysis was limited to the signals recorded within the 500 nm and 870 nm channels. Atmospheric pressure was given as the diurnal mean by the SP02-NOAA built-in sensor. Columnar ozone data were provided by the AWI team from daily ozonesonde launches. No water vapor and nitrogen dioxide absorption was taken into account, since the two above-selected channels are only negligibly affected by such gaseous absorption. All the time-series of AOD were screened for cloud attenuation effects, making use of an automated algorithm adapted from that proposed by Alexandrov et al. (2004), and described in Mazzola et al. (2010).

Fig. 2 shows the results obtained on March 28 for the two channels. As can be seen, the values recorded with the sun-tracking instruments are all within ±0.01 at 500 nm, with the exception of the ASP-15WL-ISAC sun photometer, which presented higher deviations of 0.015–0.02. Comparably differing results were obtained with this instrument on all the other days of the campaign, such AOD underestimation being due to a calibration constant underestimation, which was mainly due to non-ideal conditions, and to a lesser extent to very limited discrepancies in ROD and OOD. The AOD values given at 870 nm by the other instruments fall within a range of about 0.01, while the ASP-15WL-ISAC did not provide valid results in this channel. As expected, the AOD values determined with the various instruments become gradually more similar as *m* increases, due to the gradually weaker influence of the calibration constant (Cachorro et al., 2008). Fig. 2 also shows the AOD values obtained at 500 nm using the two MICROTOPS II sun photometers, as evaluated by the built-in instrument algorithm. Although rather scattered, they agree satisfactorily with those provided by the other instruments, differing in most cases by less than 0.01 from the centroid, which was calculated as arithmetic mean of all the measurements taken with instruments driven by sun-pointing systems.

Fig. 3 shows for each instrument the differences (hereinafter referred to as CD) between the measured values of AOD and the corresponding centroid values, determined at both 500 nm and 870 nm wavelengths as a function of *m*. Due to the high number of instruments involved in the intercomparison, and the inability to identify one instrument as master, the centroid of all AOD time series was assumed to be the actual value. Fig. 3 also shows the curves represented in the form $\pm(0.005 + 0.01/m)$ for the 500 nm

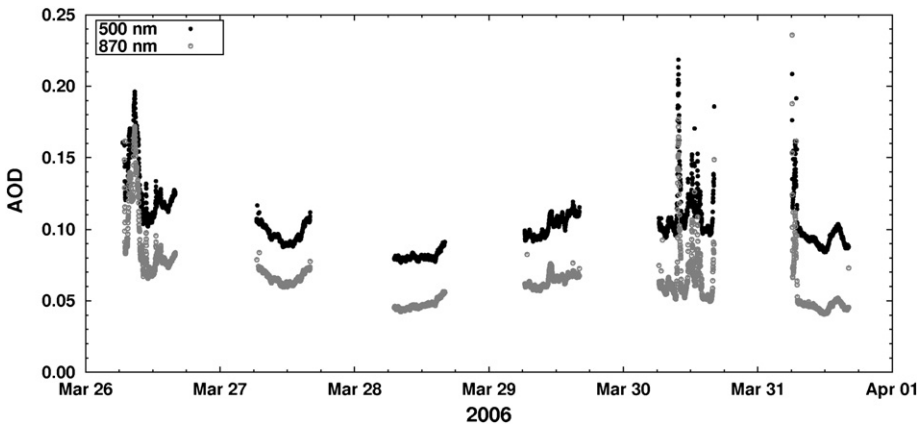

Fig. 1. Time-series of AOD at the 500 and 870 nm wavelengths determined during the Ny-Ålesund 2006 campaign, as obtained from the NOAA SP01A sun photometer measurements.

Please cite this article in press as: Mazzola, M., et al., Evaluation of sun photometer capabilities for retrievals of aerosol optical depth at high latitudes: The POLAR-AOD intercomparison campaigns, Atmospheric Environment (2011), doi:10.1016/j.atmosenv.2011.07.042

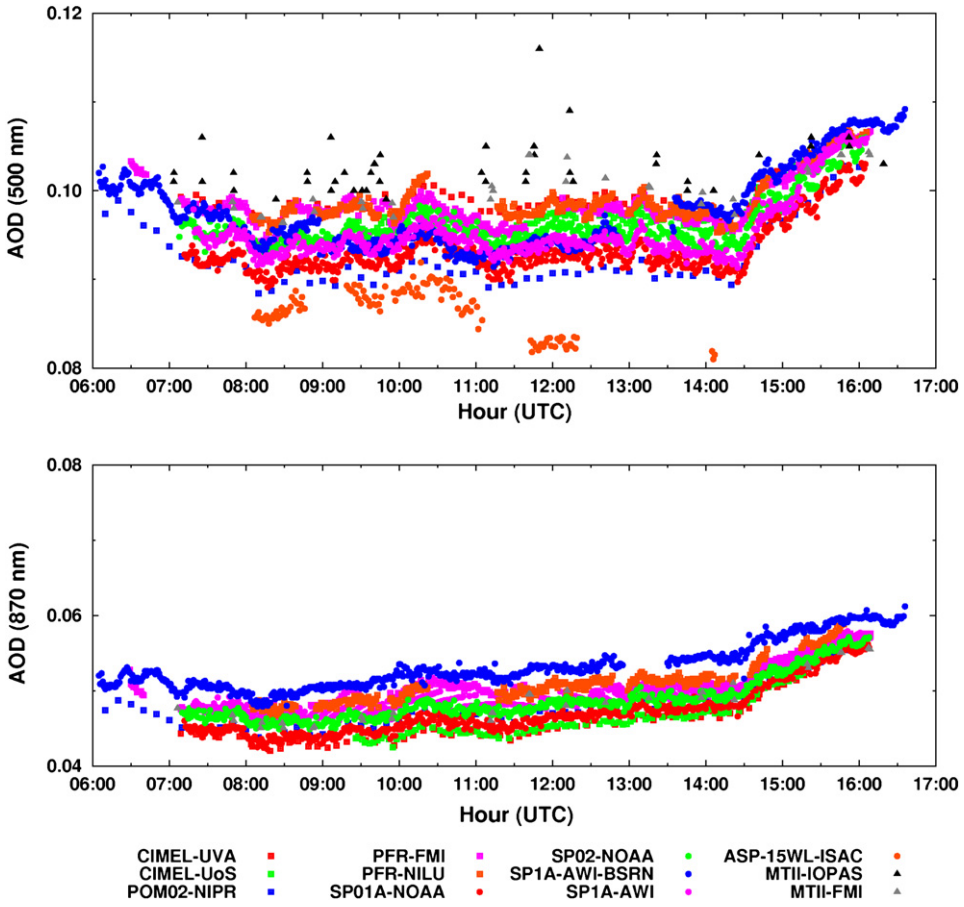

Fig. 2. Time-series of AOD at the 500 nm (upper part) and 870 nm wavelengths (lower part) as obtained on March 28, 2006, using all instruments taking part in the Ny-Ålesund campaign.

wavelength, i.e. the U_{95} limits suggested by WMO. The CD values result to be greater at low values of m for all instruments, and tend to decrease as m increases. As stated in Section 2, the AOD error is given by the sum of three terms, the first proportional to m^{-1}, and the other two independent of m (see Eq. (3)). Since common algorithms were adopted to evaluate m, $\tau_R(\lambda)$ (i.e. ROD) and $\tau_G(\lambda)$, the error affecting the results of the different instruments are expected to be constant. Furthermore, bearing in mind that the error of $J(\lambda)$ is usually small with respect to that of $J_0(\lambda)$ (Michalsky et al., 2001), the behavior of the AOD differences shown in Fig. 3 can be attributed mainly to the errors in evaluating the calibration constants of the various instruments. At 500 nm, almost all the absolute CD values are lower than 0.01 for $m < 5$, and within ± 0.005 beyond $m = 6$. Similarly, the CD values at 870 nm varied between -0.005 and 0.0075 for $m < 5$ and between -0.0025 and 0.005 for $m > 6$. Excluding those found for the ASP-15WL-ISAC sun photometer, almost all the CD values lie inside the area defined by the two hyperbolic curves at 500 nm. This implies that the WMO thresholds are fully satisfied by most of the present results.

To describe quantitatively the comparability of the AOD for the wavelength pairs of different instruments, the following statistical parameters were computed: mean bias difference (MBD), root mean square difference (RMSD), standard deviation of difference (SDD) and total uncertainty U_{95} (by combining MBD and SDD). As stated above, the results obtained for each instrument were compared to those considered as actual values (centroid). Table 2 reports the values of these parameters for each instrument and the 2 above-selected channels, together with the number of points for which they were calculated. It is shown in Table 2 that: (1) at 500 nm, excluding both the ASP-15WL-ISAC and SP1A-AWI sun photometers, MBD was found to range between -0.003 and 0.003, RMSD between 0.002 and 0.004, SSD between 0.001 and 0.003, and U_{95} between 0.003 and 0.006. The corresponding average values of RMSD, SDD and U_{95} were 0.003, 0.003 and 0.007, respectively, while the average value of MBD was found close to zero, since it is the mean difference between each instrument value and CD; (2) at 870 nm, MBD was found to vary between -0.003 and 0.004, RMSD between 0.002 and 0.004, SDD between 0.001 and 0.003 and U_{95} between 0.002 and 0.006, with overall mean values of 0.003, 0.003 and 0.005 for RMSD, SDD and U_{95}, respectively.

The above discrepancy parameters result to assume rather small values at both wavelengths, indicating that these AOD estimates are suitable for applications such as satellite validation and radiative forcing evaluations at mid-latitude sites. In addition, it is important to note that AOD (500 nm) can exhibit low values of 0.01–0.02 in the polar regions, particularly in Antarctica (Tomasi et al., 2007). For this reason, a second intercomparison campaign was planned with the principal aim of determining new updated calibration constants. The Izaña Observatory was chosen as the ideal site for such intercomparison activities, offering the advantages of high altitude, the larger range of m, and excellent facilities for the field measurements.

3.2. Izaña intercalibration campaign

Due to the frequent presence of clouds at Izaña, the daily number of coincident data was of about 300 per day on average, appreciably lower than at Ny-Ålesund. Values of AOD (500 nm) ~0.01 were

Please cite this article in press as: Mazzola, M., et al., Evaluation of sun photometer capabilities for retrievals of aerosol optical depth at high latitudes: The POLAR-AOD intercomparison campaigns, Atmospheric Environment (2011), doi:10.1016/j.atmosenv.2011.07.042

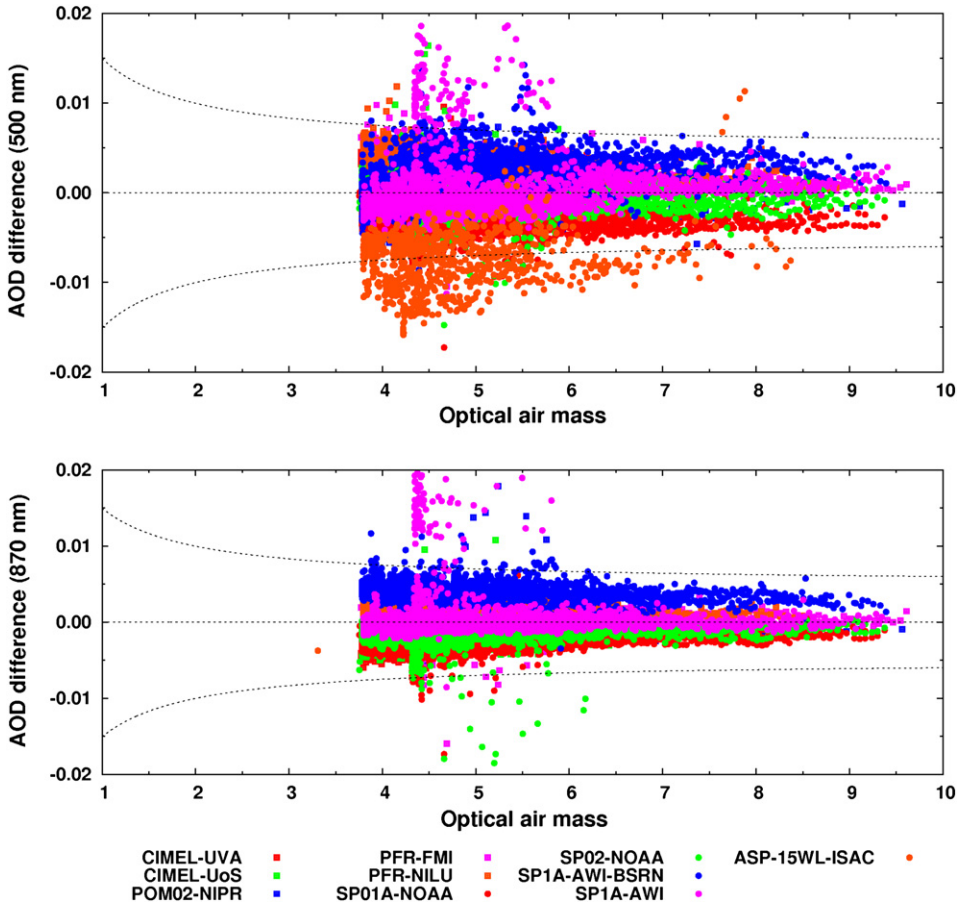

Fig. 3. AOD differences between the values provided by each instrument and the centroid of the simultaneous measurements versus the relative optical air mass, for the 500 nm channel (upper part) and the 870 nm channel (lower part), as obtained during the Ny-Ålesund campaign. Dashed lines indicate the curves of the analytical form $\pm(0.005 + 0.01/m)$.

measured on some days for the extremely clean-air conditions at this high-altitude site. A Saharan dust intrusion episode reached Izaña on October 11, causing a sharp increase in AOD up to more than 0.10 (Fig. 4).

The calibration of all the 12 sun photometers was performed following a common procedure based on the classical Langley plot method, providing values of the calibration constants that were subsequently used to evaluate the spectral values of AOD. Details on the method and the calibration results are given in Section 3.2.1.

In the analysis of the data, all the measurements performed within the channels centred at the 380, 500, 675, 870 and 1020 nm were considered, utilized by 10, 12, 9, 9 and 10 of the 12 sun photometers, respectively. It is worth mentioning that (i) the SP02-NOAA and PFR from the Finnish Meteorological Institute (FMI) sun photometers have a channel centred at 368 nm, which cannot be considered to be comparable with the 380 nm one; (ii) the nominal channel centred at 500 nm has effective peak-wavelengths ranging between 499 and 502 nm in the various instruments; (iii) the nominal channel centred at 675 nm, mounted on all instruments except for the PFR-FMI example, has peak-wavelength varying between 670 and 677 nm; (iv) most of the instruments have a channel centred at 870 nm and others at 860–862 nm; and (v)

Table 2
Comparison statistics for the results obtained by the instruments employed in the Ny-Ålesund campaign. MDB = mean bias difference = $(1/N)\sum_{i=1}^{N}(x_i - \overline{x}_i)$, RMSD = root mean square difference = $\sqrt{(1/N)\sum_{i=1}^{N}(x_i - \overline{x}_i)^2}$, SDD = standard deviation of the difference = $\sqrt{(1/(N-1))\sum_{i=1}^{N}[(x_i - \overline{x}_i) - \mathrm{MBD}]^2}$, U_{95} = 95% uncertainty = $\sqrt{\mathrm{MBD}^2 + (2\mathrm{SSD})^2}$, N = number of coincidence points.

Instrument	500 nm					870 nm				
	MBD	RMSD	SDD	U_{95}	N	MBD	RMSD	SDD	U_{95}	N
CIMEL-UVA	−0.0034	0.0036	0.0012	0.0042	326	0.0032	0.0035	0.0013	0.0041	323
CIMEL-UoS	−0.0019	0.0025	0.0016	0.0037	528	0.0029	0.0034	0.0018	0.0046	521
POM02-NIPR	0.0029	0.0034	0.0018	0.0047	299	0.0011	0.0027	0.0025	0.0051	296
PFR-FMI	−0.0023	0.0027	0.0014	0.0036	2577	−0.0008	0.0017	0.0014	0.0030	2409
PFR-NILU	−0.0032	0.0035	0.0016	0.0045	1523	−0.0017	0.0018	0.0007	0.0022	1254
SP01A-NOAA	0.0029	0.0032	0.0013	0.0039	3071	0.0025	0.0028	0.0012	0.0035	2925
SP02-NOAA	0.0002	0.0015	0.0015	0.0029	3074	0.0013	0.0019	0.0014	0.0031	2926
SP1A-AWI-BSRN	−0.0021	0.0032	0.0024	0.0052	2254	−0.0039	0.0042	0.0013	0.0048	2209
SP1A-AWI	−0.0001	0.0031	0.0031	0.0062	2350	−0.0005	0.0030	0.0030	0.0060	2253
ASP-15WL-ISAC	0.0074	0.0080	0.0031	0.0097	996	–	–	–	–	–

Please cite this article in press as: Mazzola, M., et al., Evaluation of sun photometer capabilities for retrievals of aerosol optical depth at high latitudes: The POLAR-AOD intercomparison campaigns, Atmospheric Environment (2011), doi:10.1016/j.atmosenv.2011.07.042

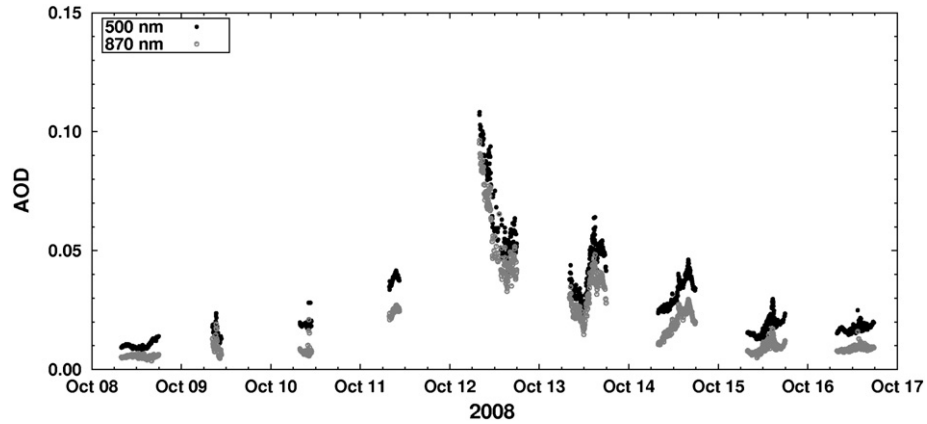

Fig. 4. Time-patterns of AOD at the 500 and 870 nm wavelengths during the Izaña campaign, as obtained from the CIMEL-327 sun photometer provided by AEROCAN.

only three instruments do not have a channel with wavelengths greater than 1000 nm. ROD and OOD were evaluated using the algorithms employed at Ny-Ålesund, considering in this case also the nitrogen dioxide absorption contribution (Berk et al., 2003).

Fig. 5 shows the values of AOD (500 nm) and AOD (870 nm) given by each instrument on October 14, 2008, characterized by a gradual increase of AOD and the presence of thin clouds around noon. The values of AOD (500 nm) and AOD (870 nm) were found to be mostly distributed within narrow ranges of ~0.01 and ~0.005, respectively. In both cases, these variability intervals were about half the Ny-Ålesund ones. The AOD values given by the MICROTOPS II from FMI are also shown in Fig. 5, with CD values lower than 0.01 at both channels.

As in Fig. 3 for the first campaign, Fig. 6 presents the CD values for each of the instruments. The range of m was from about 1.2 to more than 7 at this sub-tropical site. The scatter of data is similar to that obtained at Ny-Ålesund, with almost all the data gathered between the two uncertainty curves indicated by the WMO recommendations. The CD values were within ±0.010 for the lowest values of m and within ±0.005 for $m > 3$, while those determined for the

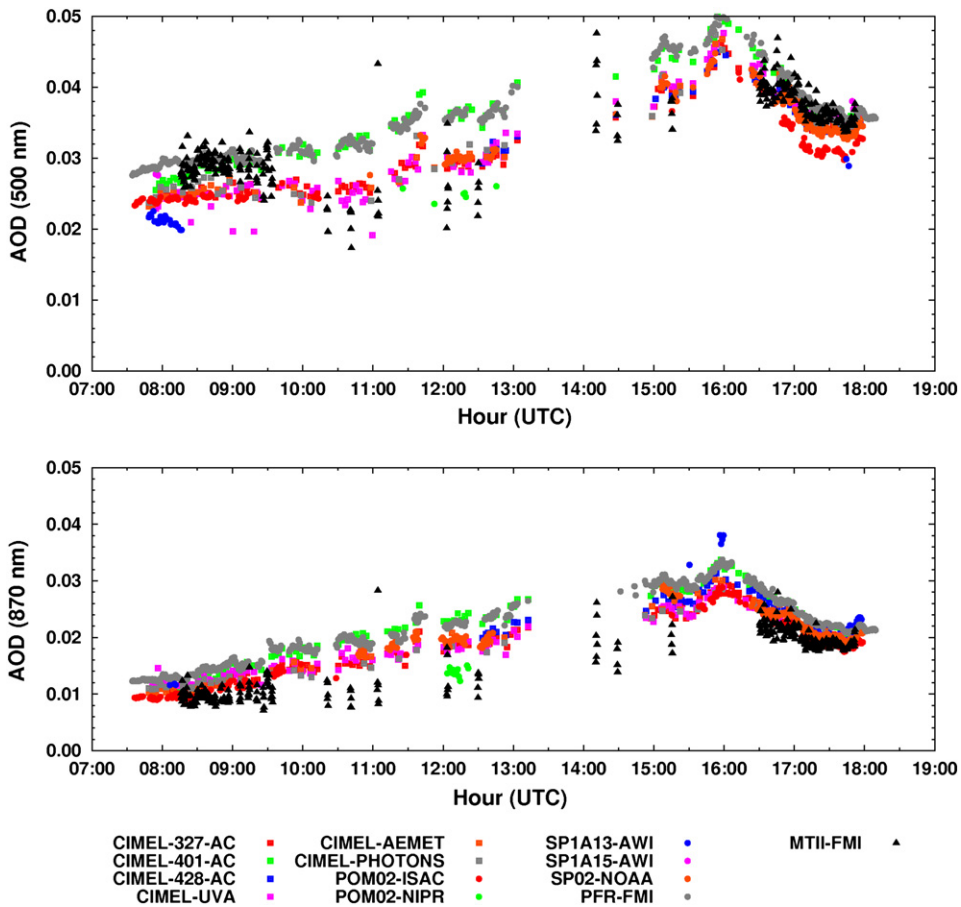

Fig. 5. AOD time-series at the 500 nm (upper part) and 870 nm (lower part) wavelengths as obtained on October 14, 2008, from all the measurements performed with the sun photometers taking part in the Izaña campaign.

Please cite this article in press as: Mazzola, M., et al., Evaluation of sun photometer capabilities for retrievals of aerosol optical depth at high latitudes: The POLAR-AOD intercomparison campaigns, Atmospheric Environment (2011), doi:10.1016/j.atmosenv.2011.07.042

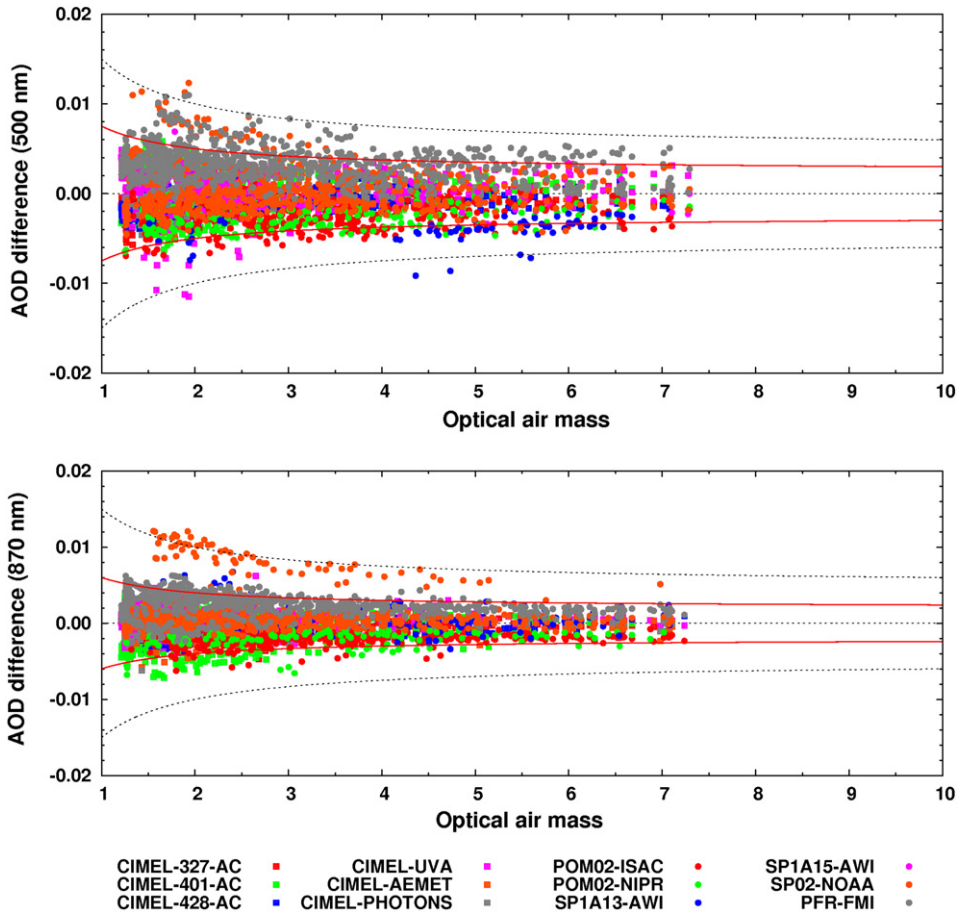

Fig. 6. As in Fig. 3, for data obtained during the Izaña campaign. Red curves show the analytical form $\pm(a + b/m)$, and are determined separately for the two 500 nm (upper part) and 870 nm (lower part) channels, assuring that at least 90% of the points fall between them.

870 nm channel are densely accumulated around zero. AOD differences varied within ±0.005 for $m \sim 1$ and decreased to about ±0.002 for $m > 4$. Numerous outliners of the NOAA-SP02 and FMI-PFR sun photometers were observed on October 11, when the AOD values gradually moved far away from the others during the first cloud-free hours in the morning. This behavior was presumably due to sun tracker problems, as well as the failure to clean away dust from the quartz entrance windows during the intrusion episode. New enveloping curves of the analytical form given by $\pm(a + b/m)$ were estimated for the 2 channels, as shown in Fig. 6. Coefficients a and b define the pair of curves containing more than 90% of the points in each unitary bin of m, with values equal to 0.005 and 0.0025 for AOD (500 nm) and 0.004 and 0.002 for AOD (870 nm), respectively.

Table 3 reports the Izaña comparison statistics defined in terms of MBD, RMSD, SDD and U_{95}. For the 500 nm channel, MBD varied between −0.004 and 0.004, RMSD between 0.001 and 0.004, SDD between 0.001 and 0.003, and U_{95} between 0.002 and 0.006. Average values of RMSD, SDD and U_{95} were equal to 0.002, 0.002 and 0.005, respectively. For the 870 nm channel, MBD varied between −0.002 and 0.002, RMSD between 0.001 and 0.004, SDD between 0.001 and 0.003 and U_{95} between 0.002 and 0.007, with average values of the last three parameters equal to 0.002, 0.002 and 0.004, respectively.

Table 3
Comparison statistics for the results obtained by the instruments employed in the Izaña campaign. MBD = mean bias difference, RMSD = root mean square difference, SDD = standard deviation of differences, U_{95} = 95% uncertainty (see caption of Table 2 for their mathematical definitions).

Instrument	500 nm					870 nm				
	MBD	RMSD	SDD	U_{95}	N	MBD	RMSD	SDD	U_{95}	N
CIMEL-327-AC	−0.0010	0.0016	0.0012	0.0025	1116	−0.0007	0.0012	0.0010	0.0021	1094
CIMEL-401-AC	0.0006	0.0025	0.0025	0.0050	1025	−0.0003	0.0025	0.0025	0.0051	989
CIMEL-428-AC	−0.0010	0.0016	0.0012	0.0027	710	−0.0007	0.0015	0.0013	0.0027	638
CIMEL-UVA	0.0002	0.0022	0.0022	0.0044	1128	0.0004	0.0013	0.0012	0.0025	1124
CIMEL-AEMET	−0.0010	0.0015	0.0011	0.0025	433	−0.0010	0.0014	0.0010	0.0022	452
CIMEL-PHOTONS	−0.0001	0.0010	0.0010	0.0021	503	−0.0002	0.0010	0.0010	0.0019	483
POM02-ISAC	−0.0027	0.0031	0.0014	0.0039	344	−0.0021	0.0023	0.0009	0.0027	363
POM02-NIPR	−0.0029	0.0031	0.0012	0.0038	164	−0.0020	0.0024	0.0012	0.0032	153
SP1A-13-AWI	−0.0039	0.0042	0.0016	0.0050	64	0.0009	0.0024	0.0022	0.0045	73
SP1A-15-AWI	0.0002	0.0017	0.0017	0.0034	63	–	–	–	–	–

Please cite this article in press as: Mazzola, M., et al., Evaluation of sun photometer capabilities for retrievals of aerosol optical depth at high latitudes: The POLAR-AOD intercomparison campaigns, Atmospheric Environment (2011), doi:10.1016/j.atmosenv.2011.07.042

3.2.1. Calibration

The Langley plot calibration method is based on the extrapolation of spectral signal $J(\lambda)$ to the extraterrestrial constant $J_0(\lambda)$ (at $m = 0$), according to the equation,

$$\ln\left[J(\lambda)R^2\right] = \ln[J_0(\lambda)] - m\tau(\lambda), \quad (4)$$

which is the linearized form of Eq. (1), obtained by applying the natural logarithm to both equation terms. Thus, the intercept of the linear best-fit of $\ln[J(\lambda)R^2]$ versus m turns out to be equal to the natural logarithm of the calibration constant $J_0(\lambda)$. To obtain reliable values of $J_0(\lambda)$, it is appropriate to consider only calibration periods presenting very stable atmospheric conditions, i.e. in presence of very limited variations in atmospheric pressure, columnar gas contents and aerosol loadings (Reagan et al., 1986). Some authors applied a refined Langley technique for the calibration of sun photometers (Schmid and Wehrli, 1995). This method consists on the use in Eq. (4) of the signal that would be measured if aerosol was the only attenuator. It can be obtained from the measured $J(\lambda)$ by removing the contributions from molecular scattering and absorption (see Eq. (2)). The corresponding slope of the fit line in this case will be AOD. Beside the use of individual air mass functions for the different attenuators, the refined Langley plot technique has the advantage that temporal changes of ROD and OOD contributing to AOD will not affect the determination of $J_0(\lambda)$, provided they can be estimated simultaneously to the measurements. During the campaign, atmospheric pressure and ambient temperature presented diurnal variations of the order of 5 hPa and 5 °C, respectively, while the columnar ozone content measured by a collocated Brewer instrument varied on average by about 5 DU on each measurement day. For these relatively small variations, ROD and OOD values were very stable throughout the calibration periods, and, hence, the classical Langley plot method was applied, while acknowledging the importance of the use of different air mass functions for different constituents, even for calibration.

In order to improve the goodness of the fit, the multi-step procedure of Harrison and Michalsky (1994) (hereinafter referred to as HM) was applied to remove the outliner data from the overall data-set, using the RMSD between the experimental points and the corresponding best-fit line as a goodness index for the results, with threshold value fixed to be equal to 0.006. Before applying the selection criteria, each original data-set was reduced by removing all the measurements taken for values of m differing by less than 0.05. In practice, the selection limits the effects due to the different acquisition rates, and, hence, to different measurement number densities. The influence of the range of m adopted for the best-fit method on the calibration results was also investigated. Calibration was performed for the three ranges 2–4, 2–5, and 2–6. Calibration was also performed for the 3 hand-held MICROTOPS II, for which the RMSD threshold was raised to 0.01, a minimum number of data points was not imposed, and the effect of the range of m on calibration results was neglected, due to the less numerous and irregular series of air mass m recorded with this sun photometer model.

Fig. 7 shows a good example of Langley plot method application for the POM02-ISAC measurements in the morning of October 16 (upper part, left). The corresponding residuals of each fit are also shown (upper part, right), all < 0.006 and randomly distributed around zero, giving RMSD lower than the HM threshold value at all wavelengths. This indicates that the Bouguer–Lambert–Beer law was valid, yielding residuals that were only due to statistical fluctuations. This is not always the case. For instance, as shown in the lower part of Fig. 7, the application of the Langley plot method to the CIMEL-UVA sun photometer measurements on the afternoon of October 14, characterized by the presence of Saharan dust, provided apparently good linear fits. However, the residuals present large fluctuations, with negative values for both low and high values of m, and positive values in the middle range. All such residuals were found in this case to assume considerably higher absolute values than those obtained on October 16, clearly indicating that the optical characteristics of the atmosphere changed appreciably during the calibration period.

On the basis of all the selection criteria, five Langley plot periods were chosen for the determination of the calibration constants: October 8 morning and afternoon, October 15 afternoon, and October 16 morning and afternoon.

The RMSD values obtained in the five calibration periods were found to be lower than the HM threshold in most cases: limiting the calculations to these Langley plot periods, the average values defined for the various spectral channels varied between 0.0005 and 0.0012 over the $2 < m < 4$ range, between 0.0008 and 0.0015 over the $2 < m < 5$ range, and between 0.0009 and 0.0015 over the $2 < m < 6$ range, generally presenting higher values at the shorter peak-wavelengths. For most of the instruments, the average value of RMSD determined over all the calibration periods increased, passing from the 2–4 to the 2–6 range of m. Such behavior confirmed that, when a longer calibration period is used, there is a higher probability of examining data characterized by a greater instability in atmospheric optical properties.

The average values of $J_0(\lambda)$ were found to be very stable. Table 4 presents such average spectral values, the values of relative standard deviation (RSD), and relative variability range (RVR) for each instrument and each of the five channels, over the three selected ranges of m. The RSD values were calculated only for the cases in which at least three valid results were achieved among the five planned Langley plots, while the values of RVR only regarded the cases with at least two valid values. RSD varied between 0.1% and 1.8%, with mean values around 1% at 380 nm and around 0.5% at the other peak-wavelengths. RVR was found to vary from 1% to 9.5%, with mean values $\sim$ 6% at 380 nm and $\sim$ 3% at the other peak-wavelengths. Table 4 clearly indicates that the stability of the calibration constants decreases in general passing from the 2–4 to the 2–6 range of m, and that the values of RSD and RVR also increase, with features similar to those of RMSD. In some cases, like those of the CIMEL sun radiometers of AEMET and PHOTONS, and the SP1A-AWI sun photometers, a lowering of the range of m to 2–4 prevented the achievement of at least three valid calibration constant values among the five, due to the very low number of available data points. At 380 nm, no valid values were obtained for the SP1A-13-AWI sun photometers, due to the high RMSD values. Finally, only the calibration constants obtained in the 2–4 range of m were adopted for determining AOD. The MICROTOPS II used by the Institute of Oceanology of the Polish Academy of Sciences (IOPAS) and by the University of Warsaw groups were not employed on these 3 days, and their Langley plot calibration was made only with data recorded from October 10 to October 13, 2008. Average values of RMSD of between 0.003 and 0.006 were found for these hand-held instruments, together with RSD of $J_0(\lambda)$ values ranging between 2.0% and 3.2%.

3.3. Ångström exponent comparison

While AOD gives a measure of columnar aerosol extinction, its spectral dependence is related to the columnar size-distribution features (Tomasi et al., 1983). The spectral dependence of AOD is usually parameterized in the form of a linear bilogarithmic relationship between AOD and wavelength λ (measured in μm), to determine the Ångström's exponent α (Ångström, 1964), although this spectral behavior is not always found in real cases (O'Neill et al., 2001). In general, this optical parameter is commonly calculated as

Please cite this article in press as: Mazzola, M., et al., Evaluation of sun photometer capabilities for retrievals of aerosol optical depth at high latitudes: The POLAR-AOD intercomparison campaigns, Atmospheric Environment (2011), doi:10.1016/j.atmosenv.2011.07.042

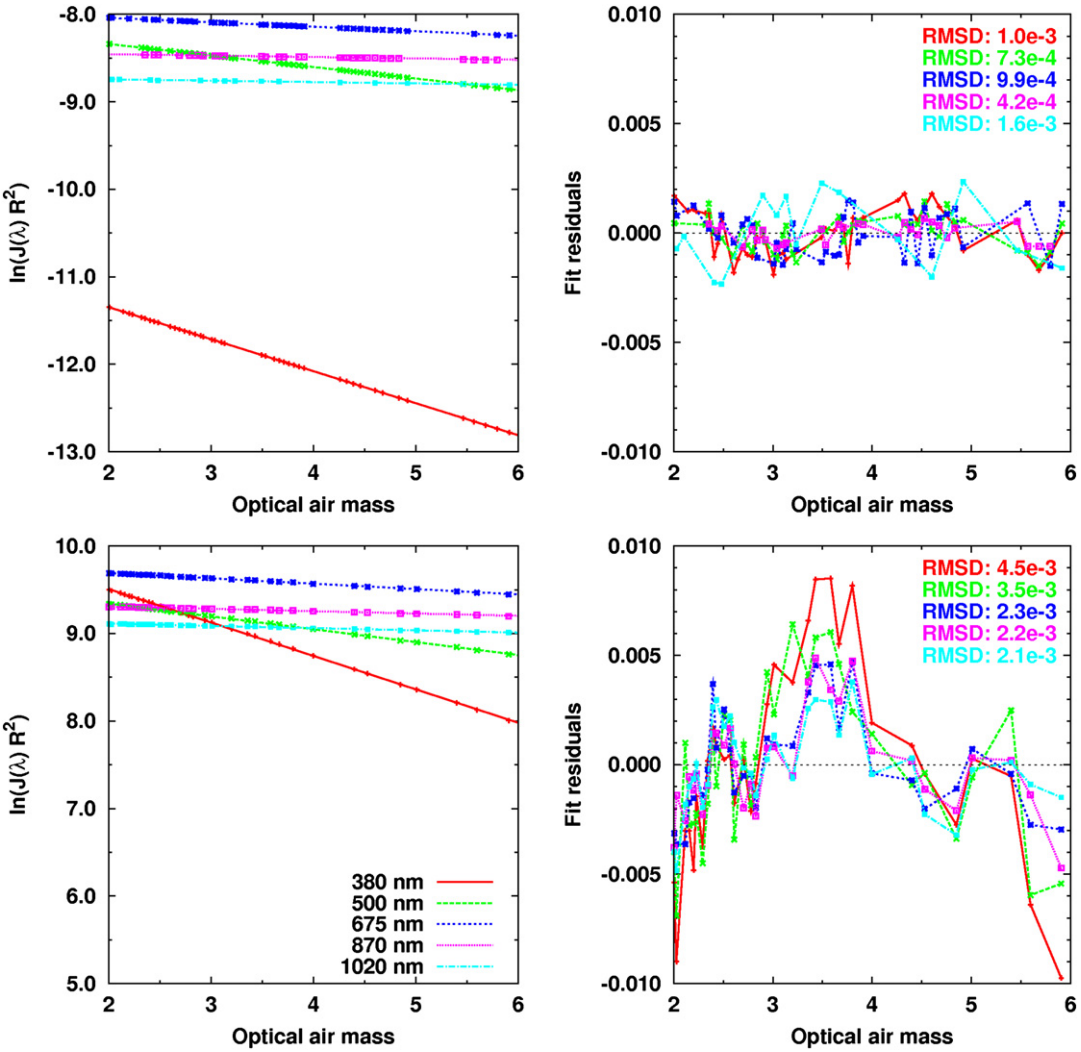

Fig. 7. Upper part: examples of the Langley plot best-fit, obtained for the 5 spectral channels of the POM02-ISAC sun photometer in the morning of October 16, 2008 (left) and corresponding residuals (right). Lower part: examples of the Langley plot best-fits, obtained for the 5 channels of the CIMEL-UVA sun photometer in the morning of October 14, 2008 (left) and corresponding residuals (right).

the slope of the line passing through two AOD-λ points over a bilogarithmic scale,

$$\alpha = -\log(\tau_2/\tau_1)/\log(\lambda_2/\lambda_1). \quad (5)$$

As suggested by WMO experts, the pair of 500 and 870 nm wavelengths was used in the present analysis.

For very low spectral values of AOD, any assessment concerning the size-distribution of columnar particles turns out to be more difficult and affected by larger uncertainties. When exponent α is evaluated for a pair of wavelengths, its relative uncertainty can be estimated as

$$|\Delta\alpha/\alpha| = |(\Delta\tau_1/\tau_1 + \Delta\tau_2/\tau_2)/\log(\tau_2/\tau_1)|, \quad (6)$$

where τ_1 and τ_2 are the values of AOD at the two wavelengths, and $\Delta\tau_i$ $(i=1, 2)$ are the corresponding absolute uncertainties. For uncertainties of AOD assumed to be equal to the above-estimated RMSD values and average values of AOD equal to 0.025 and 0.010 at the 500 and 870 nm wavelengths, respectively (c.f. Fig. 4, for example), a corresponding relative uncertainty of α equal to ~30% is obtained. Thus, for an average value of α equal to 1.5, the uncertainty turns out to be ~ 0.5, including most of the scattered values obtained on different days at various polar sites (Tomasi et al., 2007).

During the two campaigns, the daily average values of α varied between 0.8 and 1.5 at Ny-Ålesund and between 0.6 and 1.5 at Izaña, providing hourly mean values ranging between 0.51 and 1.58 and between 0.25 and 1.75, respectively. The higher variability found at Izaña probably reflects the lower range of AOD measurements observed at this high-altitude site. The differences found among the values of α obtained with the different instruments in the two campaigns were evaluated as for AOD, i.e. by comparing them with the instantaneous centroid. Fig. 8 shows the CD values of α obtained during the two campaigns as a function of AOD (500 nm). During the Ny-Ålesund campaign, the CD estimates were within ±0.25 for AOD < 0.15 and ±0.15 for higher values of AOD. At Izaña, the CD values were within ±1 for AOD < 0.025, and ±0.25 for AOD ranging between 0.025 and 0.050.

Table 5 shows a statistical comparison for α: the Ny-Ålesund results indicate that MBD varied between −0.15 and 0.07, RMSD between 0.03 and 0.16, SDD between 0.03 and 0.07 and U_{95} between 0.06 and 0.20. The corresponding Izaña values were at least 4 times higher, with MBD ranging between −0.31 and 0.52, RMSD between 0.12 and 0.78, SDD between 0.12 and 0.72 and U_{95}

Please cite this article in press as: Mazzola, M., et al., Evaluation of sun photometer capabilities for retrievals of aerosol optical depth at high latitudes: The POLAR-AOD intercomparison campaigns, Atmospheric Environment (2011), doi:10.1016/j.atmosenv.2011.07.042

Table 4
Average values, values of relative standard deviations (RSD), and values of relative variability range (RVR) for calibration constants of each instrument in the 5 channels, and for the 3 relative optical air mass ranges (n.a. means that channel was not used in the instrument).

		Optical air mass range (2–4)					Optical air mass range (2–5)					Optical air mass range (2–6)				
		380 nm	500 nm	675 nm	870 nm	1020 nm	380 nm	500 nm	675 nm	870 nm	1020 nm	380 nm	500 nm	675 nm	870 nm	1020 nm
CIMEL-327-AC	Average	23,686	25,862	22,389	23,793	13,119	23,680	25,848	22,393	23,787	13,100	23,684	25,847	22,392	23,801	13,101
	RSD (%)	1.1	0.4	0.2	0.2	0.3	1.3	0.5	0.3	0.2	0.3	1.4	0.6	0.3	0.3	0.3
	RVR (%)	5.0	2.3	1.2	1.1	2.2	6.8	2.9	1.3	1.3	2.1	7.0	3.1	1.6	1.7	2.2
CIMEL-401-AC	Average	14,174	15,768	10,564	9085.2	15,457	14,166	15,778	10,563	9086.8	15,413	14,166	15,779	10,562	9086.4	15,412
	RSD (%)	1.0	0.6	0.6	0.6	1.1	1.2	0.6	0.6	0.6	1.0	1.2	0.6	0.7	0.7	0.9
	RVR (%)	7.4	3.9	3.2	2.8	5.9	9.1	4.0	3.3	2.7	5.3	9.5	4.2	3.4	3.0	4.9
CIMEL-428-AC	Average	29,757	15,875	22,550	19,254	17,612	29,754	15,863	22,554	19,267	17,591	29,764	15,869	22,544	19,299	17,569
	RSD (%)	1.0	0.3	0.2	0.3	0.5	1.3	0.5	0.2	0.2	0.5	1.5	0.7	0.3	0.3	0.5
	RVR (%)	5.4	1.8	0.8	1.5	2.7	5.8	2.1	1.2	1.6	2.8	6.7	3.1	2.1	2.1	2.5
CIMEL-UVA	Average	29,843	15,772	18,808	11,897	9587.7	29,823	15,818	18,808	11,903	9590.1	29,830	15,825	18,803	11,905	9580.1
	RSD (%)	1.2	0.9	0.2	0.1	0.4	1.4	0.6	0.4	0.3	0.5	1.8	0.7	0.4	0.3	0.6
	RVR (%)	5.8	6.0	1.3	0.9	2.6	7.4	3.4	2.3	2.0	3.3	9.2	3.8	3.1	2.0	3.3
CIMEL-AEMET	Average	32,666	29,067	18,477	14,997	19,047	32,293	28,986	18,447	14,978	18,959	32,295	28,982	18,451	14,988	18,956
	RSD (%)	–	–	–	–	–	1.6	0.9	0.3	0.3	0.7	1.7	0.8	0.4	0.4	0.6
	RVR (%)	–	0.6	0.1	0.9	0.4	7.0	3.9	2.1	1.9	2.9	8.3	4.5	2.6	2.2	2.8
CIMEL-PHOTONS	Average	24,730	21,527	24,575	22,637	12,708	24,577	21,470	24,597	22,649	12,613	24,576	21,435	24,608	22,649	12,598
	RSD (%)	–	–	0.4	0.2	–	1.7	0.8	0.5	0.3	0.7	1.7	0.8	0.5	0.4	0.8
	RVR (%)	4.7	0.8	2.2	1.1	0.3	7.6	4.0	2.2	1.9	4.1	7.9	4.3	2.9	2.3	4.3
POM02-ISAC	Average	2.4538	31.122	35.924	22.042	16.744	2.4607	31.198	35.93	22.067	16.666	2.4656	31.231	35.94	22.087	16.667
	RSD (%)	0.9	0.4	0.1	0.2	–	0.7	0.4	0.3	0.2	0.9	0.6	0.4	0.3	0.2	0.8
	RVR (%)	4.5	2.8	0.9	1.0	1.0	3.9	2.5	1.9	1.5	5.1	3.8	2.2	2.1	1.7	4.1
POM02-NIPR	Average	2.8567	33.726	36.076	23.623	17.267	2.8603	33.743	36.092	23.641	17.29	2.856	33.779	36.09	23.65	17.282
	RSD (%)	0.3	0.4	0.3	0.4	0.3	0.9	0.6	0.5	0.5	0.3	1.2	0.7	0.6	0.6	0.4
	RVR (%)	1.7	1.5	1.2	2.1	1.5	4.4	2.8	2.6	2.6	1.5	6.2	3.7	3.1	3.1	1.5
SP1A-13-AWI	Average	–	114.39	248.29	226.5	219.38	–	114.38	248.43	228.23	219.64	–	114.76	248.5	229.2	220.39
	RSD (%)	–	0.7	0.4	–	–	–	0.9	0.1	–	0.2	–	0.8	0.2	0.3	0.4
	RVR (%)	–	3.2	1.8	2.2	0.1	–	4.0	0.6	2.4	1.0	–	4.0	0.7	1.5	1.8
SP1A-15-AWI	Average	24.443	115.19	242.44	–	118.25	–	115.45	242.85	28.55	117.37	–	115.32	242.66	27.754	114.16
	RSD (%)	–	0.1	0.7	–	–	–	0.5	0.9	–	–	–	0.6	0.9	–	–
	RVR (%)	–	0.2	3.7	–	–	–	3.1	5.1	–	–	–	4.4	5.6	–	7.0
SP02-NOAA	Average	n.a.	2387.7	1943.4	2070.2	2019.8	n.a.	2388.8	1945.9	2072	2016.2	n.a.	2388.7	1947.3	2073.5	2015.3
	RSD (%)	n.a.	0.3	0.2	0.4	0.8	n.a.	0.5	0.3	0.5	0.5	n.a.	0.5	0.3	0.5	0.4
	RVR (%)	n.a.	1.9	0.9	2.8	4.4	n.a.	2.6	2.2	3.2	3.1	n.a.	2.8	2.3	3.4	2.5
PFR-FMI	Average	n.a.	3.3616	n.a.	3.5353	n.a.	n.a.	3.3776	n.a.	3.5373	n.a.	n.a.	3.3769	n.a.	3.5332	n.a.
	RSD (%)	n.a.	0.6	n.a.	1.7	n.a.	n.a.	1.0	n.a.	1.6	n.a.	n.a.	0.9	n.a.	1.3	n.a.
	RVR (%)	n.a.	5.1	n.a.	9.4	n.a.	n.a.	6.9	n.a.	8.4	n.a.	n.a.	6.2	n.a.	7.3	n.a.

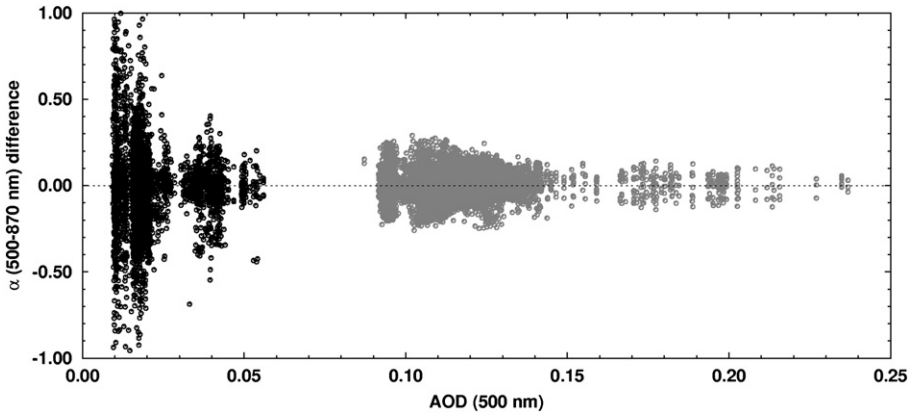

Fig. 8. Scatter plot of the difference between the Ångström parameter α given by each instrument and the centroid of the simultaneous measurements versus the average AOD obtained in the two campaigns of Ny-Ålesund (grey symbols) and Izaña (black symbols).

between 0.23 and 1.47. The overall average values of RMSD, SDD and U_{95} were estimated to be 0.06, 0.06 and 0.12 at Ny-Ålesund, and 0.39, 0.39 and 0.78 at Izaña.

4. Discussion

The results obtained during the two campaigns were compared with previous similar studies available in the literature. Comparing the results achieved by a global long-term intercomparison study with those provided by a number of shorter tests made at different wavelengths, Kim et al. (2008) evidenced that (i) the MBD values vary between −0.015 and 0.025, considering both sun photometers and hemispherical FOV radiometers, and fall within ±0.01, considering sun-pointing instruments only, and (ii) the SDD values range between about 0.001 and 0.035, with most values below 0.015. No evidence was found of a particular dependence of MBD and SDD on wavelength. The same features were also found for the U_{95} values, which varied between 0.015 and 0.070. Fig. 9 shows the scatter plots of SDD versus MBD separately for the two campaigns, as done by Kim et al. (2008) (see their Fig. 2), to give the precision of results in terms of their distance from the null values of the diagram coordinates. It is interesting to note in Fig. 9 that the ranges of SDD and MBD used by Kim et al. (2008) are ∼4–5 times wider than those found in the present analysis. For the Izaña campaign, no strong differences were evidenced among the five spectral AOD statistical parameters. The CIMEL results (labels 1–6) were more densely clustered around the null values than those of other instruments, presumably because a higher number of CIMEL instruments were employed in the campaign, with identical instrumental characteristics (FOV, tracking system, temperature control, etc.).

Table 5
Comparison statistics for the Ångström exponent α results obtained with the instruments employed in the Ny-Ålesund (upper part) and Izaña (lower part) campaigns. See Table 2 for the mathematical definition of the acronyms.

Instrument	MBD	RMSD	SDD	U_{95}	N
Ny-Ålesund					
CIMEL-UVA	−0.15	0.16	0.06	0.20	399
CIMEL-UoS	−0.12	0.14	0.07	0.18	689
POM02-NIPR	0.00	0.06	0.06	0.11	420
PFR-FMI	−0.02	0.04	0.04	0.08	3209
PFR-NILU	0.00	0.03	0.03	0.06	1324
SP01A-NOAA	−0.02	0.04	0.03	0.07	5450
SP02-NOAA	−0.03	0.04	0.03	0.06	5492
SP1A-AWI-BSRN	0.07	0.10	0.07	0.15	2805
SP1A-AWI	0.01	0.06	0.06	0.11	2910
ASP-15WL-ISAC	–	–	–	–	–
Izaña					
CIMEL-327-AC	0.01	0.14	0.14	0.27	2633
CIMEL-401-AC	−0.31	0.78	0.72	1.47	2324
CIMEL-428-AC	−0.10	0.23	0.21	0.43	1571
CIMEL-UVA	0.10	0.33	0.32	0.64	2796
CIMEL-AEMET	−0.07	0.16	0.14	0.29	1222
CIMEL-PHOTONS	0.03	0.12	0.12	0.23	1352
POM02-ISAC	−0.17	0.29	0.24	0.50	294
POM02-NIPR	0.00	0.13	0.13	0.26	137
SP1A-13-AWI	0.52	0.56	0.2	0.66	38
SP1A-15-AWI	–	–	–	–	–
SP02-NOAA	0.12	0.27	0.24	0.49	583
PFR-FMI	0.05	0.31	0.30	0.61	630

The values of the statistical parameters determined in the Ny-Ålesund comparisons were lower than the average results given in Kim et al. (2008). Comparing the Ny-Ålesund and Izaña results, it can be seen that the mean values of RMSD and SDD decreased by about 30% passing from the first to the second campaign, although the variability intervals of the statistical parameters did not change appreciably. Kim et al. (2008) pointed out that the values of SDD and RMSD are directly proportional to the mean AOD values, while a negligible correlation exists between them and MBD, the latter quantity being dependent on the instrument model. The results obtained at Ny-Ålesund are mainly due to the high values of m observed at this site during early spring, while those found at Izaña can be attributed mainly to the very low AOD values. Both situations are often observed in polar regions. The use of a common algorithm for analyzing the data allowed a reduction of the differences among the various results, this being a critical weakness in previous studies. The direct intercomparison of collocated instruments constitutes an ideal configuration that is very far from those in real networks, where even if a common algorithm can be adopted for analyzing the data, the sources of ancillary data like pressure and columnar gas contents differ considerably in most cases from one site to another.

Calibration was considered as another means of evaluating the uncertainty with which AOD is measured with sun photometry techniques. As mentioned in Section 2, errors of calibration constants affect the evaluations of AOD, contributing to the AOD error with term equal to $1/m\ [\Delta J_0(\lambda)/J_0(\lambda)]$ in Eq. (3) at each wavelength. Assuming the RSD values of $J_0(\lambda)$ as estimates of $\Delta J_0(\lambda)$, the corresponding contribution to $\Delta\tau_a(\lambda)$ turns out to be $\sim 0.01/m$ at 380 nm and $\sim 0.005/m$ in the other 4 channels. Thus, the discrepancies in AOD values evaluated at 500 nm and 870 nm turn out to be appreciably smaller than the above-estimated errors of AOD.

Please cite this article in press as: Mazzola, M., et al., Evaluation of sun photometer capabilities for retrievals of aerosol optical depth at high latitudes: The POLAR-AOD intercomparison campaigns, Atmospheric Environment (2011), doi:10.1016/j.atmosenv.2011.07.042

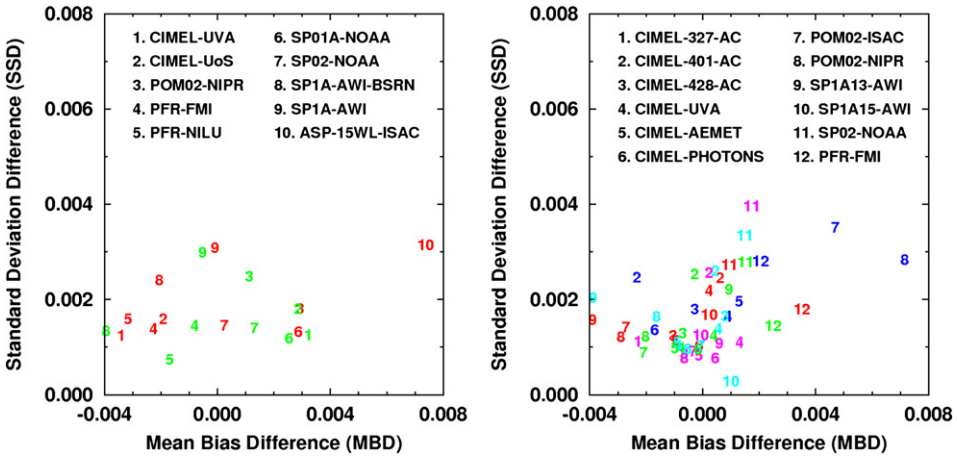

Fig. 9. Scatter plots of the standard deviation difference (SDD) in AOD versus the corresponding mean bias differences (MBD) obtained during the Ny-Ålesund (left) and Izaña campaigns (right). Colour code is used to indicate the various peak-wavelengths of the spectral channels: red = 380 nm, green = 500 nm, blue = 675 nm, violet = 870 nm, cyan = 1020 nm).

As mentioned above, the values of RMSD and SDD obtained for the AOD measurements decreased by about 30% on average passing from Ny-Ålesund to Izaña findings. In view of the much lower values of AOD measured at Izaña, presumably leading to a sharp decrease in AOD differences, the Izaña calibration seems not to have improved the comparison statistics.

Only a few intercomparison studies were found in the literature to provide useful results for the Ångström exponent α. McArthur et al. (2003) compared the results obtained with CIMEL, PFR and SP01A sun photometers through a bi-logarithmic linear least-square fit made for the common channels, over 0.03–0.35 range of AOD. They found a good agreement between PFR and SP01A results, with MBD = −0.02, and RMSD = 0.08, while the comparison of both instruments with the CIMEL sun photometer provided the worst statistics, with MBD = 0.19 and RMSD = 0.26 for the CIMEL-PFR comparison, and MBD = 0.16 and RMSD = 0.25 for the CIMEL-SP01A comparison. The differences between the results obtained from each pair of instruments decreased from absolute values of 0.4–0.8 to values lower than 0.2, as AOD increased from ~0.03 to ~0.15, and remained quite stable beyond this AOD value. The results are fully comparable with those obtained during the two POLAR-AOD intercomparison campaigns.

5. Conclusions and recommendations

Global sun photometric networks provide insufficient coverage of the polar areas, both in space and time, especially in Antarctica. In order to perform more extensive sun photometer measurements in the polar regions, with the participation of a number of research institutions, the POLAR-AOD network was set up in late 2005 and planned two sun photometer intercomparison campaigns in early spring 2006 at Ny-Ålesund and autumn 2008 at the Izaña Observatory. The results on the comparability of AOD confirmed that sun photometry is a valid technique for monitoring aerosol optical properties in the polar regions.

Mean bias differences were found not to exceed ±0.004 at all wavelengths during both campaigns, while values of RMSD and SDD equal to 0.003 were obtained in the first campaign and 0.002 in the second. Discrepancies between AOD values obtained with different instruments were found to lie within the curves of relative optical air mass m, given in the analytical form $\pm(a + b/m)$, with coefficients a and b equal to 0.005 and 0.0025 at 500 nm, and 0.004 and 0.002 at 870 nm, respectively. The values of RMSD and SDD for Ångström's exponent α were estimated to be 0.06 at Ny-Ålesund and 0.39 at Izaña.

Based on the present findings the following recommendations are confirmed, in order to maintain uncertainty and comparability standards in AOD, as required for improving the characterization of polar aerosol radiative properties:

- improve frequency and quality of calibration tests, since this is the most important factor constraining the accuracy of the final AOD values. Intercalibration campaigns can help to detect the technical problems arising from filter degradation, incorrect internal temperature compensation, and other instrumental operational defects;
- adopt common procedures for analyzing the data recorded at polar sites, including ancillary data recruitment for Rayleigh-scattering and absorption corrections (*in-situ*, satellite, climatology). This has turned out to constitute an important issue for reducing the AOD discrepancies among the results provided by the various instruments.

Acknowledgments

The Italian research activity was supported by the Programma Nazionale di Ricerche in Antartide (PNRA) and developed as a part of Subproject 2006/6.01: "POLAR-AOD: a network to characterize the means, variability and trends of the climate-forcing properties of aerosols in polar regions". The GOA-UVA group was funded by MICINN under projects CGL2008-05939-C01/CLI, CGL2009-09740 and CGL2009-09480-E. The Canadian research activity was supported by CANDAC (Canadian Network for the Detection of Atmospheric Change) and their funding organizations: CFCAS (Canadian Foundation for Climate and Atmospheric Sciences, CFI (Canadian Foundation for Innovation), NSERC (National Sciences and Engineering Research Council) and the IPY (NSERC administered) fund. Polish efforts were made within a framework of the POLAR-AOD National Grant.

References

Alexandrov, M.D., Marshak, A., Cairns, B., Lacis, A.A., Carlson, B.E., 2004. Automated cloud screening algorithm for MFRSR data. Geophysical Research Letters 31, L04118. doi:10.1029/2003GL019105.

Ångström, A., 1964. The parameters of atmospheric turbidity. Tellus 16, 64–75.

Augustine, J.A., Deluisi, J., Long, C.N., 2000. SURFRAD-a national surface radiation budget network for atmospheric research. Bulletin of the American Meteorological Society 81 (10), 2341–2357.

Berk, A., Anderson, G.P., Acharya, P.K., Hoke, M.L., Chetwynd, J.H., Bernstein, L.S., Shettle, E.P., Matthew, M.W., Adler-Golden, S.M., 2003. MODTRAN4 Version 3 Revision 722 1 User's Manual.

Bodhaine, B.A., Wood, N.B., Dutton, E.G., Slusser, J.R., 1999. On Rayleigh optical depth calculations. Journal of Atmospheric and Oceanic Technology 16, 1854–1861.

Cachorro, V.E., Toledano, C., Sorribas, M., Berjón, A., de Frutos, A.M., Laulainen, N., 2008. An "in situ" calibration–correction procedure (KCICLO) based on AOD diurnal cycle: comparative results between AERONET and reprocessed (KCICLO method) AOD-alpha data series at El Arenosillo, Spain. Journal of Geophysical Research 113, D02207. doi:10.1029/2007JD009001.

Dubovik, O., King, M.D., 2000. A flexible inversion algorithm for retrieval of aerosol optical properties from Sun and sky radiance measurements. Journal of Geophysical Research 105 (D16), 20673–20696. doi:10.1029/2000JD900282.

Forster, P., Ramaswamy, V., Artaxo, P., Berntsen, T., Betts, R., Fahey, D.W., Haywood, J., Lean, J., Lowe, D.C., Myhre, G., Nganga, J., Prinn, R., Raga, G., Schulz, M., Van Dorland, R., 2007. Changes in atmospheric constituents and in radiative forcing. In: Solomon, S., Qin, D., Manning, M., Chen, Z., Marquis, M., Averyt, K.B., Tignor, M., Miller, H.L. (Eds.), Climate Change 2007: The Physical Science Basis. Contribution of Working Group I to the Fourth Assessment Report of the Intergovernmental Panel on Climate Change. Cambridge University Press, Cambridge, United Kingdom and New York, NY, USA.

Fröhlich, C., Shaw, G.E., 1980. New determination of Rayleigh scattering in the terrestrial atmosphere. Applied Optics 19 (11), 1773–1775.

Harrison, L., Michalsky, J., 1994. Objective algorithms for the retrieval of optical depths from ground-based measurements. Applied Optics 33, 5126–5132.

Herber, A., Thomason, L.W., Gernandt, H., Leiterer, U., Nagel, D., Schulz, K.H., Kaptur, J., Albrecht, T., Notholt, J., 2002. Continuous day and night aerosol optical depth observations in the Arctic between 1991 and 1999. Journal of Geophysical Research 107 (D10), 4097. doi:10.1029/2001JD000536.

Holben, B.N., Eck, T.F., Slutsker, I., Tanré, D., Buis, J.P., Setzer, A., Vermote, E., Reagan, J.A., Kaufman, Y.J., Nakajima, T., Lavenu, F., Jankowiak, I., Smirnov, A., 1998. AERONET – a federal instrument network and data archive for aerosol characterization. Remote Sensing of Environment 66, 1–16.

Holben, B.N., Tanré, D., Smirnov, A., Eck, T.F., Slutsker, I., Abuhassan, N., Newcomb, W.W., Schafer, J., Chatenet, B., Lavenue, F., Kaufman, Y.J., Vande Castle, J., Setzer, A., Markham, B., Clark, D., Frouin, R., Halthore, R., Karnieli, A., O'Neill, N.T., Pietras, C., Pinker, R.T., Voss, K., Zibordi, G., 2001. An emerging ground-based aerosol climatology: aerosol optical depth from AERONET. Journal of Geophysical Research 106 (D11), 12067–12097.

International Organization for Standardization, 1995. Guide to the Expression of Uncertainty in Measurement, ISBN 92-67-101889.

Kim, D.H., Sohn, B.J., Nakajima, T., Takamura, T., Takemura, T., Choi, B.C., Yoon, S.C., 2004. Aerosol optical properties over east Asia determined from ground-based sky radiation measurements. Journal of Geophysical Research 109, D02209. doi:10.1029/2003JD003387.

Kim, S.W., Yoon, S.C., Dutton, E.G., Kim, J., Wehrli, C., Holben, B.N., 2008. Global surface-based sun photometer network for long-term observations of column aerosol optical properties: intercomparison of aerosol optical depth. Aerosol Science and Technology 42 (1), 1–9.

Mazzola, M., Lanconelli, C., Lupi, A., Busetto, M., Vitale, V., Tomasi, C., 2010. Columnar aerosol optical properties in the Po Valley, Italy, from MFRSR data. Journal of Geophysical Research 115, D17206. doi:10.1029/2009JD013310.

McArthur, L.J.B., Halliwell, D.H., Niebergall, O.J., O'Neill, N.T., Slusser, J.R., Wehrli, C., 2003. Field comparison of network Sun photometers. Journal of Geophysical Research 108 (D19), 4596. doi:10.1029/2002JD002964.

Michalsky, J.J., Schlemmer, J.A., Berkheiser, W.E., Berndt, J.L., Harrison, L.C., Laulainen, N.S., Larson, N.R., Barnard, J.C., 2001. Multiyear measurements of aerosol optical depth in the Atmospheric Radiation Measurement and Quantitative Links programs. Journal of Geophysical Research 106, 12099–12107. doi:10.1029/2001JD900096.

Mitchell, R.M., Forgan, B.W., 2003. Aerosol measurement in the Australian outback: intercomparison of sun photometers. Journal of Atmospheric and Oceanic Technology 20, 54–66.

O'Neill, N.T., Eck, T.F., Holben, B.N., Smirnov, A., Dubovik, O., Royer, A., 2001. Bimodal size distribution influences on the variation of Angstrom derivatives in spectral and optical depth space. Journal of Geophysical Research 106, 9787–9806. doi:10.1029/2000JD900245.

Ortiz de Galisteo, J.P., Toledano, C., Cachorro, V., Rodríguez, E., de Frutos, A., 2008. Analysis of aerosol optical depth evaluation in polar regions and associated uncertainties. Advances in Science and Research 2, 5–8. doi:10.5194/asr-2-5-2008.

Reagan, J.A., Thomason, L.W., Herman, B.M., Palmer, J.M., 1986. Assessment of atmospheric limitations on the determination of the solar spectral constant from ground-based spectroradiometer measurements. IEEE Transactions on Geoscience and Remote Sensing GE-24 (2), 258–266. doi:10.1109/TGRS.1986.289645.

Rozwadowska, A., Sobolewski, P., 2010. Variability in aerosol optical properties at Hornsund, Spitsbergen. Oceanologia 52 (4), 599–620.

Schmid, B., Wehrli, C., 1995. Comparison of Sun photometer calibration by use of the Langley technique and the standard lamp. Applied Opticts 34, 4500–4512.

Schmid, B., Michalsky, J., Halthore, R., Beauharnois, M., Harrison, L., Livingston, J., Russell, P., Holben, B.N., Eck, T., Smirnov, A., 1999. Comparison of aerosol optical depth from four solar radiometers during the fall 1997 ARM intensive observation period. Geophysical Research Letters 26 (17), 2725–2728. doi:10.1029/1999GL900513.

Shaw, G.E., Stamnes, K., Hu, Y.X., 1993. Arctic haze: perturbation to the radiation field. Meteorology and Atmospheric Physics 51 (3), 227–235. doi:10.1007/BF01030496.

Smirnov, A., Holben, B.N., Giles, D.M., Slutsker, I., O'Neill, N.T., Eck, T.F., Macke, A., Croot, P., Courcoux, Y., Sakerin, S.M., Smyth, T.J., Zielinski, T., Zibordi, G., Goes, J.I., Harvey, M.J., Quinn, P.K., Nelson, N.B., Radionov, V.F., Duarte, C.M., Losno, R., Sciare, J., Voss, K.J., Kinne, S., Nalli, N.R., Joseph, E., Krishna Moorthy, K., Covert, D.S., Gulev, S.K., Milinevsky, G., Larouche, P., Belanger, S., Horne, E., Chin, M., Remer, L.A., Kahn, R.A., Reid, J.S., Schulz, M., Heald, C.L., Zhang, J., Lapina, K., Kleidman, R.G., Griesfeller, J., Gaitley, B.J., Tan, Q., Diehl, T.L., 2011. Maritime aerosol network as a component of AERONET – first results and comparison with global aerosol models and satellite retrievals. Atmospheric Measurements Techniques 4, 583–597. doi:10.5194/amt-4-583-2011.

Stone, R.S., 2002. Monitoring aerosol optical depth at Barrow, Alaska and South Pole; Historical overview, recent results, and future goals. In: Colacino, M. (Ed.), Proceedings of the 9th Workshop Italian Research on Antarctic Atmosphere, Rome, Italy, 22–24 October 2001. Ital. Phys. Soc., Bologna, Italy, pp. 123–144.

Tomasi, C., Caroli, E., Vitale, V., 1983. Study of the relationship between Ångström's wavelength exponent and Junge particle size distribution exponent. Journal of Climate and Applied Meteorology 22, 1707–1716.

Tomasi, C., Vitale, V., Petkov, B., Lupi, A., Cacciari, A., 2005. Improved algorithm for calculations of Rayleigh-scattering optical depth in standard atmospheres. Applied Optics 44, 3320–3341.

Tomasi, C., Vitale, V., Lupi, A., Di Carmine, C., Campanelli, M., Herber, A., Treffeisen, R., Stone, R.S., Andrews, E., Sharma, S., Radionov, V., von Hoyningen-Huene, W., Stebel, K., Hansen, G.H., Myhre, C.L., Wehrli, C., Aaltonen, V., Lihavainen, H., Virkkula, A., Hillamo, R., Ström, J., Toledano, C., Cachorro, V., Ortiz, P., de Frutos, A., Blindheim, S., Frioud, M., Gausa, M., Zielinski, T., Petelski, T., Yamanouchi, T., 2007. Aerosols in polar regions: a historical overview based on optical depth and in situ observations. Journal of Geophysical Research 112, D16205. doi:10.1029/2007JD008432.

Wehrli, C., 2000. Calibrations of filter radiometers for determination of atmospheric optical depth. Metrologia 37, 419–422. doi:10.1088/0026-1394/37/5/16.

WMO, 2005. WMO/GAW Experts Workshop on a Global Surface-based Network for Long Term Observations of Column Aerosol Optical Properties, in: WMO TD No. 1287, Davos, Switzerland, 8–10 March 2004, 153 pgs.

Please cite this article in press as: Mazzola, M., et al., Evaluation of sun photometer capabilities for retrievals of aerosol optical depth at high latitudes: The POLAR-AOD intercomparison campaigns, Atmospheric Environment (2011), doi:10.1016/j.atmosenv.2011.07.042